

# Simulation of Magnetospheric Sawtooth Oscillations: the Role of Kinetic Reconnection in the Magnetotail

Xiantong Wang<sup>1</sup>, Yuxi Chen<sup>1,2</sup>, Gábor Tóth<sup>1</sup>

<sup>1</sup>Department of Climate and Space Sciences and Engineering, University of Michigan, Ann Arbor, MI, USA

<sup>2</sup>Now at Princeton Plasma Physics Laboratory, Princeton University, Princeton, NJ, USA

## Key Points:

- The kinetic physics in the MHD with embedded particle-in-cell model plays an important role in reproducing sawtooth oscillations
- Kinetic reconnection in the magnetotail can produce sawtooth-like oscillations without varying ionospheric outflow

---

Corresponding author: Xiantong Wang, [xtwang@umich.edu](mailto:xtwang@umich.edu)

This is the author manuscript accepted for publication and has undergone full peer review but has not been through the copyediting, typesetting, pagination and proofreading process, which may lead to differences between this version and the [Version of Record](#). Please cite this article as [doi: 10.1029/2022GL099638](https://doi.org/10.1029/2022GL099638).

This article is protected by copyright. All rights reserved.

## Abstract

Magnetospheric sawtooth oscillations are observed during strong and steady solar wind driving conditions. The simulation results of our global MHD model with embedded kinetic physics show that when the total magnetic flux carried by constant solar wind exceeds a threshold, sawtooth-like magnetospheric oscillations are generated. Different from previous works, this result is obtained without involving time-varying ionospheric outflow in the model. The oscillation period and amplitude agree well with observations. The simulated oscillations cover a wide range of local times, although the distribution of magnitude as a function of longitude is different from observations. Our comparative simulations using ideal or Hall MHD models do not produce global time-varying features, which suggests that kinetic reconnection physics in the magnetotail is a major contributing factor to sawtooth oscillations.

## Plain Language Summary

The magnetospheric sawtooth oscillation is a global-scale phenomenon in the Earth's magnetosphere. Observations and simulations suggest that the oxygen outflow from the ionosphere is inducing the sawtooth oscillations by affecting the rate of the magnetic reconnection: a fundamental physical process converting magnetic energy to plasma energy. We use a model where the magnetic reconnection is solved by kinetic physics and show that sawtooth-like oscillations can be induced if the incoming solar wind magnetic flux exceeds a threshold. This work proposes a new mechanism contributing to magnetospheric sawtooth oscillations.

## 1 Introduction

More than two decades ago, Belian et al. (1995) observed giant quasi-periodic, global flux variations with periods of 2 to 4 hours through the Los Alamos National Laboratory energetic particle detectors, CPA (Charged Particle Analyzer), and the time variations of electron fluxes at geosynchronous orbit resemble a tooth of a saw blade: a slow decrease followed by a rapid increase (Henderson, 2004). Moreover, this feature is observed in a wide range of magnetic local time (MLT), which distinguishes it from isolated substorms. These periodic injections also have impacts on other geospace features like magnetic field variations at geosynchronous orbit, the auroral electrojet index, and the polar cap index (Cai et al., 2006; Henderson, Reeves, et al., 2006; Henderson, Skoug, et al., 2006; Huang et al., 2003). Although there is still no definitive answer to the mechanisms producing the sawtooth oscillations, numerical simulations for the coupled magnetosphere-ionosphere system have demonstrated a possible explanation related to the  $O^+$  outflow from the ionosphere (Brambles et al., 2011). The basic idea of this theory is that the periodic mass loading and unloading from the ionospheric outflow alters the reconnection rate in the magnetotail current sheet. The different reconnection rate results in different magnetic field configuration in the tail, which modulates the ionospheric outflow rate. This feed back loop produces the periodic oscillations.

There are a number of studies establishing this theory over the past decade. Wiltberger et al. (2010) uses the Multi-Fluid Lyon Fedder Mobarrry (MFLFM) model to demonstrate that the out-flowing cusp ions transported to the tail can have an effect on the magnetic configuration. and trigger substorm dipolarizations. Yu and Ridley (2013) also shows that cusp  $O^+$  outflow can influence the development of isolated substorms. Brambles et al. (2011) applies an empirical power-law relationship between the Alfvénic Poynting flux and the resulting ionospheric outflow flux at the simulation inner boundary and shows that this outflow can induce quasi-periodic substorms resembling observed sawtooth oscillations. In a follow-up study, Ouellette et al. (2013) studies how the ion composition of the plasma sheet and magnetotail affects the tail reconnection rate. They hypothesized that the massive outflow inflates the magnetosphere and enables the development

62 of the next sawtooth oscillation. Later on, Brambles et al. (2013) used the same model  
 63 on two different types of sawtooth events induced by different external driving conditions:  
 64 the Stream Interaction Region (SIR)-driven 24 October 2002 event and the Coronal Mass  
 65 Ejection (CME)-driven 18 April 2002 event. They find that quasi-periodic substorms oc-  
 66 curred in the SIR event without outflow while no periodic substorm occurs in the CME  
 67 event without outflow. Presumably, the quasi-periodic substorms in the SIR event are  
 68 triggered by the variations in the external driving condition while in the CME event, they  
 69 are more related to the internal mechanism of the magnetosphere. More recently, Lund  
 70 et al. (2018) uses mass composition data from the Cluster satellites and discovers the  
 71 role ionospheric outflow plays in inducing sawtooth oscillations. They find during the  
 72 CME events, the  $O^+$  in the mid-tail plasma sheet is mostly from the cusp/dayside while  
 73 the nightside outflow preconditions the plasma sheet to enable the sawtooth oscillations.  
 74 The recent work by Zhang et al. (2020) illustrates that magnetospheric sawtooth oscil-  
 75 lations can be solely induced by cusp  $O^+$  outflows in the global simulation conducted  
 76 by the LFM model.

77 The previous publications all show that the magnetotail reconnection is the key fac-  
 78 tor in inducing the sawtooth oscillations and the ionospheric outflow is affecting the re-  
 79 connection rate. In this paper, we use the University of Michigan’s Space Weather Mod-  
 80 eling Framework (SWMF) (Tóth et al., 2012) to investigate how kinetic reconnection af-  
 81 fects the sawtooth oscillations under constant solar wind driving conditions. In addition  
 82 to the global MHD model simulating Earth’s magnetosphere, we are using the FLEKS  
 83 (Flexible Exascale Kinetic Simulator) (Chen et al., 2021) in the magnetotail to model  
 84 the tail reconnection with full kinetic physics. For comparison, we also present results  
 85 by pure ideal MHD and Hall MHD models to emphasize the significance of the kinetic  
 86 effects. Different from the previous work discussed above, we are not varying the plasma  
 87 outflow from the ionosphere, hence the periodic oscillations observed are caused by the  
 88 kinetic reconnection process embedded into the global MHD model.

89 The model description and simulation setup are described in section 2, the simu-  
 90 lation results are presented in section 3 and we conclude in section 4.

## 91 2 Model Description and Simulation Setup

92 The simulations presented in this paper are conducted with the magnetohydrody-  
 93 namics with embedded particle-in-cell (MHD-EPIC) model (Daldorff et al., 2014; Chen  
 94 & Tóth, 2019). The MHD-EPIC model two-way couples the BATS-R-US MHD code (Powell  
 95 et al., 1999; Tóth et al., 2008) and the semi-implicit particle-in-cell code FLEKS (Chen  
 96 et al., 2021) through the Space Weather Modeling Framework (Tóth et al., 2012). The  
 97 global magnetosphere structure is simulated by an ideal MHD model, with an embed-  
 98 ded PIC region in the magnetotail to simulate the kinetic physics in the magnetic recon-  
 99 nection. The ionospheric electrodynamics is simulated by the Ridley Ionosphere Model  
 100 (RIM) (Ridley et al., 2004) that solves a Poisson-type equation for the electric poten-  
 101 tial on a 2-D spherical grid, which is used to set the  $\mathbf{E} \times \mathbf{B}$  velocity at the inner bound-  
 102 ary of BATS-R-US. The MHD-EPIC model has been applied in studying multiple plan-  
 103 etary and moon magnetospheres, such as the Earth (Chen et al., 2017, 2020), Mars (Ma  
 104 et al., 2018), Mercury (Chen et al., 2019) and Ganymede (Tóth et al., 2016; Zhou et al.,  
 105 2019, 2020).

106 A three-dimensional block-adaptive Cartesian grid of BATS-R-US is used to cover  
 107 the entire computational domain:  $-224R_E < x < 32R_E$  and  $-128R_E < y, z < 128R_E$   
 108 in GSM coordinates. The grid resolution is  $1/4 R_E$  between  $-60R_E < x < 20R_E$ ,  $-20R_E <$   
 109  $y < 20R_E$  and  $-16R_E < z < 16R_E$ . A shell region near the Earth from  $2.5 R_E$  to  
 110  $3.5 R_E$  is covered with  $1/8 R_E$  grid resolution. The PIC box, the computational domain  
 111 of FLEKS, is in the magnetotail between  $-80R_E < x < -4R_E$ ,  $-20R_E < y < 20R_E$   
 112 and  $-10R_E < z < 10R_E$  with grid resolution  $1/4 R_E$ . Figure 1 shows a 3-D overview

of the simulation domain at  $t = 3600$  s from the simulation presented in this paper. The color contour is the mass density on the equatorial plane, and the magnetic field lines of two flux ropes are also plotted in the magnetotail. The black box is the PIC domain, which covers the tail region where magnetic reconnection could happen.

To reduce the computational cost and make the simulation feasible, the speed of light  $c$  is reduced to 15,000 km/s to speed up the convergence of the implicit solver, and the ion-electron mass ratio  $m_i/m_e$  is decreased to 100 to increase the electron kinetic scales. These modification have no direct impact on the results at the ion and global scales. In addition to these numerical adjustments, we also scale up the ion and electron mass per charge by a factor of 16 to increase the ion inertial length so that it can be resolved with an affordable grid resolution. The ion inertial length in the magnetotail is larger than about  $1 R_E$  with the scaling factor applied, which can be marginally resolved by the  $1/4 R_E$  grid resolution. Tóth et al. (2017) presents theoretical arguments and numerical experiments and concludes that (1) the solution of the equations is not sensitive to the scaling at global scales and (2) the solution at the kinetic scale is proportional to the scaling factor but will look the same. The global scale features, including sawtooth oscillations, are not affected by the scaling factor.

The dipole tilt angle is set to  $0^\circ$  to form an idealized case. The inner boundary of BATS-R-US is at  $r = 2.5 R_E$ , where the density is fixed at 28 amu/cc, the radial velocity is set to 0, and the tangential velocity is calculated from the ionospheric  $\mathbf{E} \times \mathbf{B}$  drift. Floating (zero-gradient) boundary condition is set for temperature and the magnetic field  $\mathbf{B}_1$  that is the difference between the total field and the dipole. This boundary condition does not prescribe ionospheric outflow, although plasma density is maintained at around 28 amu/cc and will be accelerated due to the external motional electric field in the open cusp region.

The solar wind condition applied at the inflow boundary of BATS-R-US is set to constant to study the magnetosphere's response to an idealized ICME solar wind driving. We have two solar wind conditions: a)  $V_x = -600$  km/s, IMF  $B_z = -15$  nT for strong driving and b)  $V_x = -400$  km/s, IMF  $B_z = -5$  nT for weak driving. The plasma number density and the temperature of the solar wind are fixed at  $5 \text{ cm}^{-3}$  and  $10^5$  K, respectively. The solar wind velocity components  $V_y, V_z$  and IMF components  $B_x, B_y$  are all set to 0. Both strong and weak driving conditions are applied to the MHD-EPIC model to demonstrate that exceeding a threshold of the transported magnetic flux from the solar wind is necessary for triggering the sawtooth oscillation. We also run Hall MHD and ideal MHD models under strong driving to emphasize the importance of the kinetic reconnection. The Hall region, which covers the same simulation domain as the PIC region, is embedded in an ideal MHD simulation. We also apply the scaling factor 16 to the Hall MHD model. All three models are using the same grid in BATS-R-US.

We first run BATS-R-US and RIM for 15,000 steps using local time stepping with ideal MHD until the system reaches a quasi-steady state. Then the time accurate mode is turned on for 12 hours of physical time. The FLEKS model and/or the Hall MHD solver are switched on in the time accurate section.

### 3 Results

#### 3.1 Occurrence of sawtooth-like oscillations

A characteristic signature of sawtooth oscillations is the temporal variation of the magnetic inclination angle, which is defined as the angle  $\alpha = \arcsin(|B_z|/B)$  between the magnetic field vector and the equatorial plane. Here  $B_z$  and  $B$  are the local magnetic field  $Z$  component and magnitude, respectively. The change of the magnetic inclination angle results from the field line stretching and dipolarization processes. At the geostationary orbit, the average minimum inclination angle of an observed sawtooth is

163 26° as compared to 43° for the isolated substorms (Cai et al., 2006). Figure 2(a) shows  
 164 the magnetic inclination angles observed at  $r = 8 R_E$  radial distance from the center  
 165 of Earth, 9° latitude and 2 am magnetic local time (MLT). The corresponding GSM co-  
 166 ordinates are  $[x, y, z] = [-6.93, -4, 1.25] R_E$ . Compared to the geostationary orbit, we  
 167 are observing further toward the magnetotail because the variations detected at  $6.6 R_E$   
 168 are small. Due to the  $\pm Z$  symmetry, the inclination angle is 90° in the equatorial plane,  
 169 so we extract values slightly above that plane. As we will see later, the largest variation  
 170 of the inclination angle occurs slightly off from the midnight direction, this is why we  
 171 chose 2 am MLT.

172 The dashed gray line is the result of the ideal MHD model with strong solar wind  
 173 driving, and the simulated magnetosphere takes about 2 hours to converge to a steady  
 174 solution. There is no perturbation of the inclination angle, which stays at about 50° for  
 175 the entire simulation. The solid gray line shows the result from the Hall MHD model with  
 176 strong solar wind driving, which takes about 1.5 hours to reach a quasi-steady state. How-  
 177 ever, unlike the ideal MHD model, the inclination angle oscillates around 60° with a  $\pm 5^\circ$   
 178 range. The difference in the average inclination angles between the ideal MHD and Hall  
 179 MHD models can be explained by the different reconnection modes resulting from the  
 180 two models. Simulations show that the ideal MHD gives a Sweet-Parker type solution  
 181 while the Hall MHD model gives a solution closer to the Petschek type (Murphy et al.,  
 182 2009). Though they are different in the values of inclination angles, it is clear that there  
 183 are no sawtooth-like oscillations in the ideal and Hall MHD simulation results.

184 The MHD-EPIC result with strong solar wind driving is shown by the solid red line,  
 185 while the result of weak solar wind driving is plotted in green. The MHD-EPIC run with  
 186 weak solar wind driving shows similar oscillation to the Hall MHD run, although with  
 187 a smaller average inclination angle around 55°. The MHD-EPIC run with strong solar  
 188 wind driving shows different inclination angle variations from the other three runs. Af-  
 189 ter about four hours of the simulation, the inclination angle drops to about 30° from 55°  
 190 with a recovering phase afterward. There are three sawteeth shown in Figure 2 (a) and  
 191 their starting times are marked by dashed vertical lines at  $t = 4.15\text{h}, 5.38\text{h}$  and  $7.15\text{h}$ .  
 192 The third sawtooth shows a small dipolarization during the stretching phase. Partial dipo-  
 193 larizations are consistent with observations as shown in the bottom panel of the figure.  
 194 Panels (b) and (c) of Figure 2 compare the time variation of  $B_z$  from the MHD-EPIC  
 195 simulation with strong solar wind driving and the observation from the POLAR satel-  
 196 lite of the sawtooth event reported by Pulkkinen et al. (2006). The POLAR satellite tra-  
 197 jectory is around  $x = -8.0 R_E$  and  $y = 3.5 R_E$  and moves from  $-2 R_E$  to  $2 R_E$  in GSM  
 198 coordinate. The absolute values of  $B_z$  are different between the simulation and the ob-  
 199 servation because they are acquired at different positions, but the differences between  
 200 the maximum and the minimum  $B_z$  for each sawtooth are around 40 nT in both. Fur-  
 201 thermore, a partial dipolarization was observed by POLAR between 17 : 00 and 18 :  
 202 00 UT that is reminiscent of the simulation results between 9 and 10 hours.

203 From the four simulations with different setups presented in this section, we can  
 204 conclude that two essential factors need to be satisfied for a global model to generate sawtooth-  
 205 like oscillations without the time varying ionospheric outflow. First, the total eroded mag-  
 206 netic flux  $\Phi_{MP} = \int_t v^{4/3} B_T^{2/3} \sin^{8/3}(\theta_c/2) dt$  needs to exceed a certain threshold, where  
 207  $t$  [s] is the duration of the stretching phase,  $v$  [m/s] is the solar wind velocity,  $B_T$  [T] is  
 208 the transverse field and  $\theta_c$  is the IMF clock angle. Cai and Clauer (2013) report a thresh-  
 209 old value  $10^6$  Wb from multiple sawtooth events. The  $\Phi_{MP}$  from the strong and weak  
 210 solar wind conditions in our simulations are  $3.1 \times 10^5$  Wb and  $1.1 \times 10^6$  Wb, respec-  
 211 tively with an estimated value  $t = 1$  hour. The observed threshold falls between these  
 212 two solar wind conditions. Second, the tail reconnection needs to be simulated by the  
 213 kinetic model.

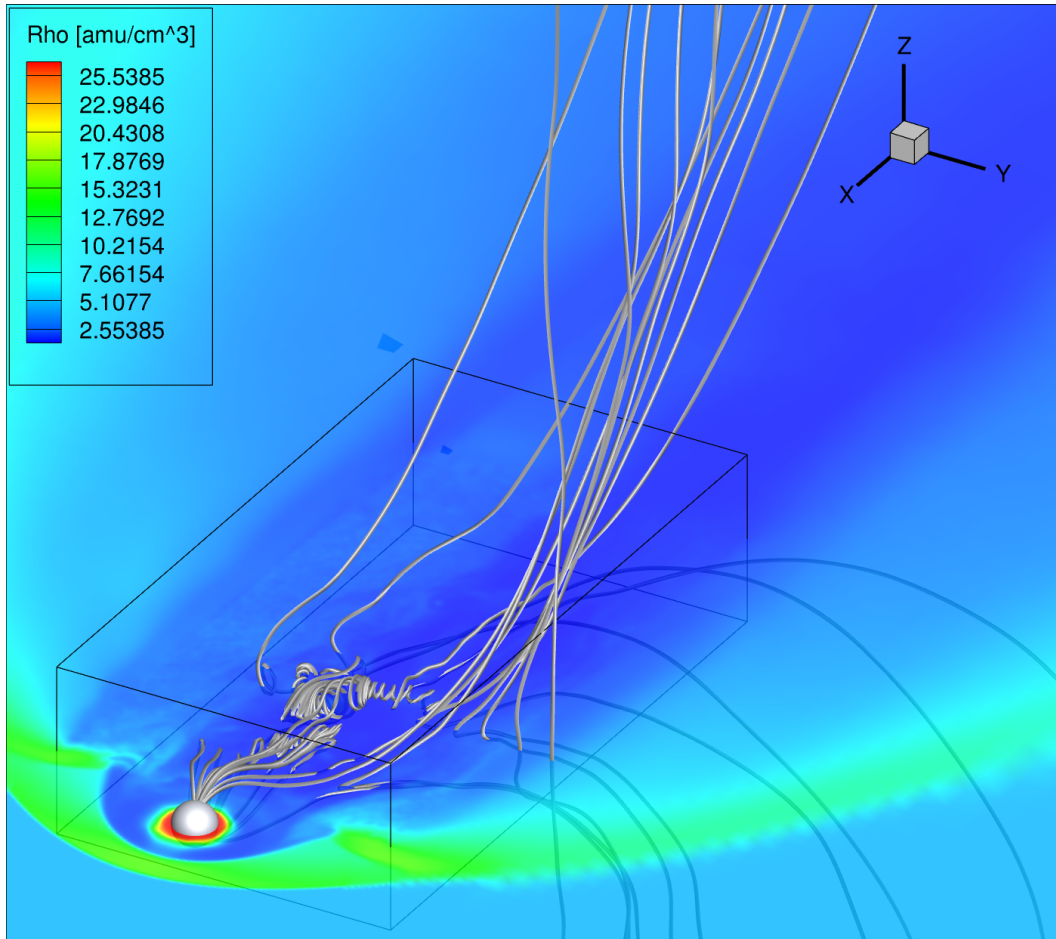


**Figure 1.** The global structure of Earth's magnetosphere at simulation time  $t = 1$  h from the MHD-EPIC simulation with the strong solar wind driving condition. The color contour shows the mass density in the equatorial plane. The white spherical surface is the inner boundary at  $2.5 R_E$ . The gray rods are magnetic field lines of two flux ropes in the magnetotail. The black box is the domain of the PIC model that covers potential magnetic reconnection sites in the tail.

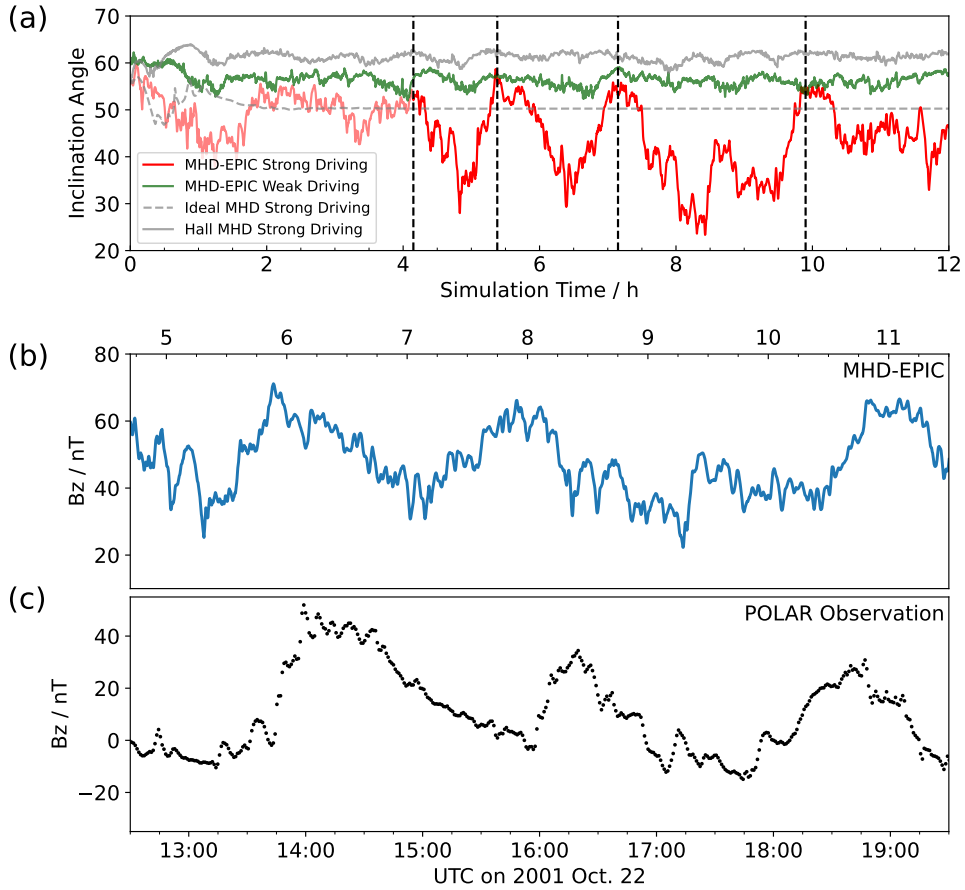


**Figure 2.** (a) Magnetic inclination angle plots from multiple simulations. MHD-EPIC with strong and weak solar wind driving conditions are shown in red and green. For comparison, the ideal and Hall MHD results under strong solar wind driving are also plotted in dashed and solid gray, respectively. All inclination angles are taken at the same position:  $x = -6.93 R_E$ ,  $y = -4 R_E$  and  $z = 1.25 R_E$ . (b) Time variation of  $B_z$  at the same position from the MHD-EPIC simulation with strong driving. (c) Sawtooth event observations of  $B_z$  by the POLAR satellite from  $(-8.0, 3.5, -2) R_E$  to  $(-8.0, 3.5, 2) R_E$  in GSM coordinate. (Figure 3 from Pulkkinen et al. (2006)).

214

### 3.2 Kinetic reconnection and sawtooth-like oscillations

215

216

217

218

219

220

221

In this subsection, we will investigate the connection between the sawtooth-like oscillations shown in Figure 2 and the kinetic reconnection process in the magnetotail. Panel (a) of Figure 3 shows the magnetic field, particle energy, and half of the total energy inside the PIC box normalized by the total energy at  $t = 2$  h. The electric field energy oscillates around 0.06% percent of the total energy, which is negligible compared to the energy of the magnetic field and the particles. The magnetic field and particles have a periodic energy gain/loss accompanied with the sawtooth oscillations.

222

223

224

225

226

227

228

229

230

231

232

233

234

235

236

237

238

239

240

241

242

243

244

245

246

247

248

Before  $t = 4.4$  h, there is no substantial energy transferred between the magnetic field and the particles. At  $t \approx 4.4$  h, the  $E_{\text{magnetic}}$  starts increasing while the  $E_{\text{particle}}$  starts decreasing. This stretching phase (S1) ends at  $t \approx 5$  h when the difference reaches about 10%. In the next dipolarization phase (D1) the energy is transferred back from the magnetic field to the particles. The two parts of energy recover to the initial state at  $t \approx 5.4$ h, which ends the first sawtooth period, and a similar oscillation starts at  $t \approx 6$  h and ends at  $t \approx 7.5$  h (S2 and D2). Panels (b)-(e) of Figure 3 depict the electron kinetic energy multiplied by the sign of the  $X$  component of the electron velocity that is defined as  $K_e = \frac{1}{2}\rho_e u_e^2 \text{sgn}(u_{e,x})$ . The  $K_e$  values are plotted on the  $B_x = 0$  isosurface, which is the middle of the tail current sheet. We choose the electron kinetic energy because the electron features are well localized, and the sign change of  $K_e$  accurately indicates the position of the reconnection X line. The two blue vertical lines labeled S1 and S2 in panel (a) are marked at  $t = 4$ h 48min and  $t = 6$ h 30min when  $E_{\text{magnetic}}$  reaches the maximum in each period and their corresponding  $E_k$  contour plots are shown in panels (b) and (d). In these panels, the magnetosphere is in a "stretching phase", when the X lines move towards the distant tail at  $x \approx -40 R_E$ . Another two red vertical lines labeled D1 and D2 in panel (a) are marked at  $t = 5$ h 14min and  $t = 7$ h 01min. Those two lines mark when  $E_{\text{particle}}$  (or  $E_{\text{magnetic}}$ ) is increasing (or decreasing) most rapidly. Panels (c) and (e) show the corresponding  $E_k$  contour plots, when the magnetosphere is in a "dipolarization phase." In this phase, the X line is observed at  $x \approx -15 R_E$  and the  $E_k$  near the X line is much larger. The "dipolarization phase" is also matching the recovery from the minimum inclination angle observed in Figure 2. The third sawtooth oscillation in the simulation is more complicated than the previous two. The dipolarization phase is interrupted by a secondary stretching from  $t \approx 8$ h 36min to  $t \approx 9$ h 24min. The third oscillation fully recovers to the initial state at  $t \approx 10$  h. The period of the oscillations varies from 1.5 h to 3 h, which is very comparable with the observed periodicity.

249

### 3.3 Spatial distribution of the magnetic inclination angle

250

251

252

253

254

255

256

257

258

259

260

261

262

263

The wide extension of the variations of magnetic inclination angles in magnetic local time (MLT) is a critical signature of the sawtooth oscillations. Figure 4 shows the magnetic inclination contour plot from the MHD-EPIC simulation with strong solar wind driving conditions. The inclination angle is calculated along the circle  $\sqrt{x^2 + y^2} = 7.9 R_E$  in the plane  $z = 1.26 R_E$  (the inclination angle is  $90^\circ$  in the  $z = 0$  plane due to the symmetry of this idealized setup). The location we are looking at is further from the center of Earth than the observations at the geosynchronous orbit reported by Cai et al. (2006). Our MHD-EPIC simulation does not produce strong magnetic field perturbations at geosynchronous orbit. Despite the difference in the locations, the simulated inclination angle distribution over MLT exhibits several similarities compared to the observations. The minimum inclination angle from dawn to dusk is about  $17^\circ$ , which is close to observed sawtooth oscillations. The broad span in MLT also agrees with the observation. The stretching and dipolarization phases with a period of around 1.5 hours are close to the observed periodicity.



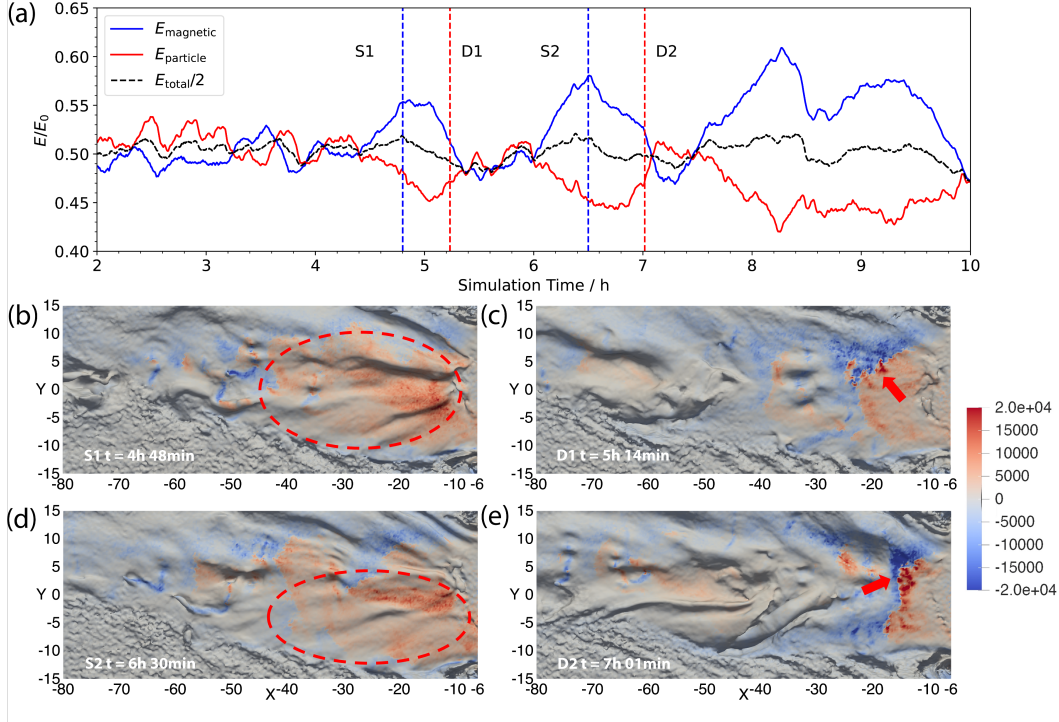


**Figure 3.** (a) The integrated magnetic field energy (blue) and particle energy (red) inside the PIC region normalized by the total energy at  $t=2\text{h}$ . The black line shows half of the normalized total energy. The four dashed vertical lines correspond to the times depicted by panels (b)-(e), respectively, during the stretching (S1 and S2) and dipolarization (D1 and D2) phases. The stretching and dipolarization regions are highlighted by red circles and arrows, respectively. These plots show the color contours of the electron kinetic energy multiplied by the sign of the  $X$  component of the electron velocity:  $K_e = \frac{1}{2}\rho_e u_e^2 \text{sgn}(u_{e,x})$ . The color contour is plotted on the  $B_x = 0$  isosurface that identifies the middle of the magnetotail current sheet. Sharp jumps from dark blue to dark red color indicate reconnection jets emanating from the X-lines. The black shadows show that the current sheet surface is rippled.

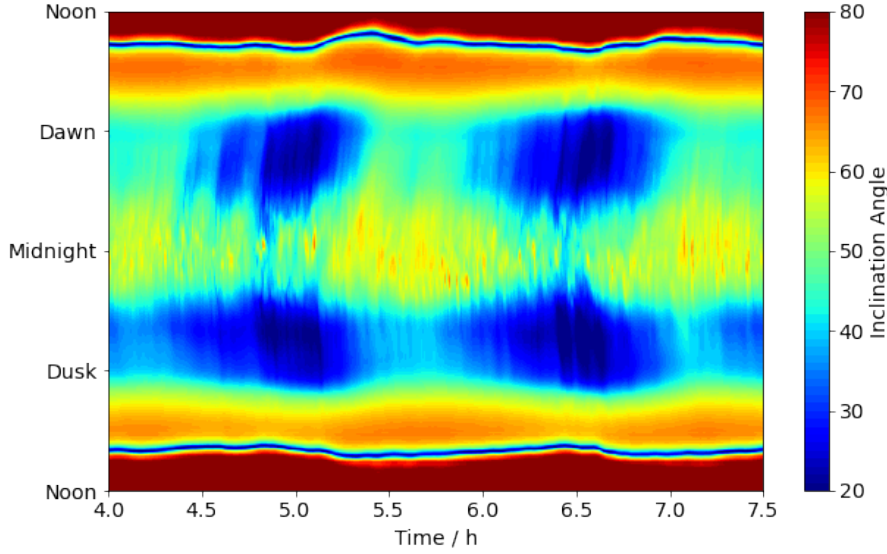


**Figure 4.** The contour plot of the magnetic inclination angle of the first two sawteeth from the MHD-EPIC simulation with strong solar wind driving. The inclination angle is evaluated on the circle  $\sqrt{x^2 + y^2} = 7.9 R_E$  in the plane  $z = 1.26 R_E$ , which is outside the geosynchronous orbit.

264 While many features of the MHD-EPIC simulation results agree reasonably well  
 265 with observations of sawtooth events (Cai et al., 2006), there are also several discrep-  
 266 ancies. First, the signatures at the geosynchronous orbit are not strong enough to be ob-  
 267 served, indicating that the stretching and dipolarization in the model are less energetic  
 268 than in reality. Second, the stretching at midnight is much weaker than at dawn and dusk  
 269 in the simulation. This is the reason why the inclination angle in Figure 2 is extracted  
 270 at 2 am MLT. The observed sawtooth oscillations exhibit the lowest inclination angle  
 271 near midnight and expand towards dawn and dusk. Third, the duration of each sawtooth  
 272 from the MHD-EPIC simulation varies from 1.5 to 3 hours, which is slightly shorter than  
 273 a typically observed sawtooth that lasts from 2-4 hours.

274 One possible reason for the weaker signatures at midnight is that the "critical level"  
 275 of the accumulated magnetic flux simulated by the MHD-EPIC model is lower than re-  
 276 ality at dawn and dusk. The reconnection that happens there first causes stronger dipol-  
 277 arization at dawn and dusk than observed, which dissipates the accumulated magnetic  
 278 flux and preempts strong dipolarization at midnight.

## 279 4 Conclusion and Discussion

280 In this paper, we use the MHD with Embedded Particle-In-Cell (MHD-EPIC) model  
 281 to study the role kinetic reconnection plays in generating magnetospheric sawtooth events.  
 282 The PIC region covers a box region in the magnetotail where the reconnection could po-  
 283 tentially happen. Different from prior MHD simulations of sawtooth events, there is no  
 284 time varying ionospheric outflow transporting plasma to the magnetotail. We apply both  
 285 strong and weak solar wind driving conditions in the MHD-EPIC simulations to demon-  
 286 strate that the occurrence of the sawtooth oscillations depends on the incoming rate of  
 287 the magnetic flux from the solar wind. To emphasize the significance of the kinetic model,

288 we also perform the simulation using ideal MHD and Hall MHD models with the strong  
289 solar wind driving conditions for comparison.

290 We examine the temporal variation of the magnetic inclination angle in the near  
291 tail at  $(x, y, z) = (-6.93, -4, 1.25) R_E$  from different simulations. We find that only the  
292 MHD-EPIC model with strong solar wind driving condition produces periodic oscilla-  
293 tions of the magnetic inclination angle that has a minimum value below  $30^\circ$ , which demon-  
294 strates that both the kinetic magnetic reconnection and the incoming rate of the mag-  
295 netic flux from the solar wind are essential to induce the sawtooth oscillations. We in-  
296 vestigate the variations of magnetic and particle energy from the MHD-EPIC simula-  
297 tion. The energy is transferred from the particles to the magnetic field during the stretch-  
298 ing phase. When the dipolarization starts, the energy transfers in the opposite direction.  
299 We also plot the electron kinetic energy contour on the current sheet surface, and we ob-  
300 serve that the dipolarization phase of the sawtooth oscillation is related to the forma-  
301 tion of a reconnection X-line close to the Earth, which is consistent with observations  
302 (Henderson, 2004). We find that the oscillations from the MHD-EPIC simulation exhibit  
303 a wide span over the magnetic local time that is a signature of observed sawtooth events.  
304 However, there are three major discrepancies between the MHD-EPIC generated saw-  
305 tooth oscillations and the observations: 1. the signature at the geosynchronous orbit is  
306 relatively weak. 2. the simulated period of the sawtooth oscillations varies from 1.5 to  
307 3 hours that is somewhat shorter than the observed periods of 2 to 4 hours. 3. the min-  
308 imum inclination angle in the simulation is found at the dawn and dusk regions rather  
309 than at midnight.

310 We suggest that the kinetic reconnection in the magnetotail can solely reproduce  
311 the periodic loading and unloading process of the magnetic flux in the magnetosphere.  
312 The kinetic model can accumulate the magnetic flux beyond a critical level on the night-  
313 side, which then triggers dipolarization. This process is recognized as the direct caus-  
314 ing mechanism of the sawtooth oscillations (Zhang et al., 2020). However, the ideal and  
315 Hall MHD models yield lower thresholds for dissipating the magnetic flux through nu-  
316 merical diffusion-driven reconnection. Thus those models cannot produce sawtooth-like  
317 oscillations. Hence we conclude that in addition to the ionospheric outflow, the sawtooth  
318 oscillations might be an intrinsic feature of the kinetic reconnection in the magnetotail  
319 when the incoming magnetic flux from the solar wind exceeds a threshold. However, the  
320 discrepancies between the observation and the MHD-EPIC simulation suggest that iono-  
321 spheric outflow is also an important factor. The ionospheric  $O^+$  transported into the mag-  
322 netotail will change the plasma mass density and composition, which may make the stretch-  
323 ing phase last longer. Also, the "preconditioning" by the nightside outflow mentioned  
324 by Zhang et al. (2020) might reduce the discrepancy at the midnight sector between the  
325 MHD-EPIC simulation and observations. In future work, we believe it is important to  
326 include both ionospheric outflow and kinetic magnetic reconnection physics in the mag-  
327 netotail to fully understand sawtooth oscillations.

## 328 Open Research

329 The POLAR satellite data is obtained from the Coordinated Data Analysis Web  
330 (CDAWeb) from NASA (<https://cdaweb.gsfc.nasa.gov>). The SWMF code (including BATS-  
331 R-US and FLEKS) is publicly available through the website ([https://clasp.engin.umich.edu/research/theory-  
332 computational-methods/swmf-downloadable-software/](https://clasp.engin.umich.edu/research/theory-computational-methods/swmf-downloadable-software/)) after registration. The simula-  
333 tion output and scripts used for generating figures in this paper can be obtained online  
334 (<https://doi.org/10.7302/61te-2903>) through the University of Michigan's Deep Blue Data  
335 repository, which is specifically designed for U-M researchers to share their research data  
336 and to ensure its long-term viability.

## Acknowledgments

This work was primarily supported by NSF PRE-EVENTS grant No. 1663800. We also acknowledge support from the NASA DRIVE Center at the University of Michigan under grant NASA 80NSSC20K0600. We acknowledge the Texas Advanced Computing Center (TACC) at The University of Texas at Austin for providing HPC and storage resources that have contributed to the research results reported within this paper.

## References

- Belian, R., Cayton, T., & Reeves, G. (1995). Quasi-periodic global substorm generated flux variations observed at geosynchronous orbit. *Space plasmas: Coupling between small and medium scale processes*, 86, 143–148.
- Brambles, O., Lotko, W., Zhang, B., Ouellette, J., Lyon, J., & Wiltberger, M. (2013). The effects of ionospheric outflow on icme and sir driven sawtooth events. *Journal of Geophysical Research: Space Physics*, 118(10), 6026–6041.
- Brambles, O., Lotko, W., Zhang, B., Wiltberger, M., Lyon, J., & Strangeway, R. (2011). Magnetosphere sawtooth oscillations induced by ionospheric outflow. *Science*, 332(6034), 1183–1186.
- Cai, X., & Clauer, C. (2013). Magnetospheric sawtooth events during the solar cycle 23. *Journal of Geophysical Research: Space Physics*, 118(10), 6378–6388.
- Cai, X., Clauer, C., & Ridley, A. (2006). Statistical analysis of ionospheric potential patterns for isolated substorms and sawtooth events. *Ann. Geophys.*, 24, 1977.
- Chen, Y., & Tóth, G. (2019). Gauss's law satisfying energy-conserving semi-implicit particle-in-cell method. *J. Comput. Phys.*, 386, 632. doi: 10.1016/j.jcp.2019.02.032
- Chen, Y., Tóth, G., Cassak, P., Jia, X., Gombosi, T. I., Slavin, J., ... Peng, B. (2017). Global three-dimensional simulation of earth's dayside reconnection using a two-way coupled magnetohydrodynamics with embedded particle-in-cell model: initial results. *J. Geophys. Res.*, 122, 10318. doi: 10.1002/2017JA024186
- Chen, Y., Toth, G., Zhou, H., & Wang, X. (2021). Fleks: A flexible particle-in-cell code for multi-scale plasma simulations. *Earth and Space Science Open Archive*. doi: doi.org/10.1002/essoar.10508070.1
- Chen, Y., Tth, G., Hietala, H., Vines, S. K., Zou, Y., Nishimura, Y., ... Markidis, S. (2020). Magnetohydrodynamic with embedded particle-in-cell simulation of the geospace environment modeling dayside kinetic processes challenge event. *Earth and Space Science*, 7(11), e2020EA001331. Retrieved from <https://agupubs.onlinelibrary.wiley.com/doi/abs/10.1029/2020EA001331> doi: <https://doi.org/10.1029/2020EA001331>
- Chen, Y., Tth, G., Jia, X., Slavin, J. A., Sun, W., Markidis, S., ... Raines, J. M. (2019). Studying dawn-dusk asymmetries of mercury's magnetotail using mhd-epic simulations. *Journal of Geophysical Research: Space Physics*, 124(11), 8954–8973.
- Daldorff, L. K. S., Tóth, G., Gombosi, T. I., Lapenta, G., Amaya, J., Markidis, S., & Brackbill, J. U. (2014). Two-way coupling of a global Hall magnetohydrodynamics model with a local implicit Particle-in-Cell model. *J. Comput. Phys.*, 268, 236. doi: 10.1016/j.jcp.2014.03.009
- Henderson, M. (2004). The may 2–3, 1986 cdaw-9c interval: A sawtooth event. *Geophysical research letters*, 31(11).
- Henderson, M., Reeves, G., Skoug, R., Thomsen, M., Denton, M. H., Mende, S., ... Singer, H. (2006). Magnetospheric and auroral activity during the 18 april 2002 sawtooth event. *Journal of Geophysical Research: Space Physics*, 111(A1).
- Henderson, M., Skoug, R., Donovan, E., Thomsen, M., Reeves, G., Denton, M. H.,

- 390 ... others (2006). Substorms during the 10–11 august 2000 sawtooth event.  
 391 *Journal of Geophysical Research: Space Physics*, 111(A6).
- 392 Huang, C.-S., Reeves, G., Borovsky, J., Skoug, R., Pu, Z., & Le, G. (2003). Periodic  
 393 magnetospheric substorms and their relationship with solar wind variations.  
 394 *Journal of Geophysical Research: Space Physics*, 108(A6).
- 395 Lund, E. J., Nowrouzi, N., Kistler, L. M., Cai, X., & Frey, H. U. (2018). On the role  
 396 of ionospheric ions in sawtooth events. *Journal of Geophysical Research: Space  
 397 Physics*, 123(1), 665–684.
- 398 Ma, Y., Russell, C. T., Toth, G., Chen, Y., Nagy, A. F., Harada, Y., ... others  
 399 (2018). Reconnection in the martian magnetotail: Hall-mhd with embedded  
 400 particle-in-cell simulations. *Journal of Geophysical Research: Space Physics*,  
 401 123(5), 3742–3763.
- 402 Murphy, N., Sovinec, C., & Cassak, P. (2009). Simulation and analysis of magnetic  
 403 reconnection in an experimental geometry. In *Bulletin of the american astro-  
 404 nomical society* (Vol. 41, p. 514).
- 405 Ouellette, J., Brambles, O., Lyon, J., Lotko, W., & Rogers, B. (2013). Properties  
 406 of outflow-driven sawtooth substorms. *Journal of Geophysical Research: Space  
 407 Physics*, 118(6), 3223–3232.
- 408 Powell, K., Roe, P., Linde, T., Gombosi, T., & De Zeeuw, D. L. (1999). A solution-  
 409 adaptive upwind scheme for ideal magnetohydrodynamics. *J. Comput. Phys.*,  
 410 154, 284–309. doi: 10.1006/jcph.1999.6299
- 411 Pulkkinen, T., Ganushkina, N. Y., Tanskanen, E., Kubyshkina, M., Reeves, G.,  
 412 Thomsen, M., ... Gjerloev, J. (2006). Magnetospheric current systems during  
 413 stormtime sawtooth events. *Journal of Geophysical Research: Space Physics*,  
 414 111(A11).
- 415 Ridley, A., Gombosi, T., & Dezeew, D. (2004, February). Ionospheric control of the  
 416 magnetosphere: conductance. *Annales Geophysicae*, 22, 567–584. doi: 10.5194/  
 417 angeo-22-567-2004
- 418 Tóth, G., Chen, Y., Gombosi, T. I., Cassak, P., Markidis, S., & Peng, B. (2017).  
 419 Scaling the ion inertial length and its implications for modeling reconnection in  
 420 global simulations. *J. Geophys. Res.*, 122, 10336. doi: 10.1002/2017JA024189
- 421 Tóth, G., Jia, X., Markidis, S., Peng, B., Chen, Y., Daldorff, L., ... Dorelli, J.  
 422 (2016). Extended magnetohydrodynamics with embedded particle-in-cell  
 423 simulation of ganymede’s magnetosphere. *J. Geophys. Res.*, 121. doi:  
 424 10.1002/2015JA021997
- 425 Tóth, G., Ma, Y. J., & Gombosi, T. I. (2008). Hall magnetohydrodynamics on block  
 426 adaptive grids. *J. Comput. Phys.*, 227, 6967–6984. doi: 10.1016/j.jcp.2008.04  
 427 .010
- 428 Tóth, G., van der Holst, B., Sokolov, I. V., Zeeuw, D. L. D., Gombosi, T. I., Fang,  
 429 F., ... Opher, M. (2012). Adaptive numerical algorithms in space weather  
 430 modeling. *J. Comput. Phys.*, 231, 870–903. doi: 10.1016/j.jcp.2011.02.006
- 431 Wiltberger, M., Lotko, W., Lyon, J. G., Damiano, P., & Merkin, V. (2010). In-  
 432 fluence of cusp o+ outflow on magnetotail dynamics in a multifluid mhd  
 433 model of the magnetosphere. *J. Geophys. Res.*, 115(A10), 148–227. doi:  
 434 10.1029/2010JA015579
- 435 Yu, Y., & Ridley, A. J. (2013). Exploring the influence of ionospheric o+ outflow on  
 436 magnetospheric dynamics: dependence on the source location. *Journal of Geo-  
 437 physical Research: Space Physics*, 118(4), 1711–1722.
- 438 Zhang, B., Brambles, O. J., Lotko, W., & Lyon, J. G. (2020). Is nightside outflow  
 439 required to induce magnetospheric sawtooth oscillations. *Geophysical Research  
 440 Letters*, 47(6), e2019GL086419.
- 441 Zhou, H., Tóth, G., Jia, X., & Chen, Y. (2020). Reconnection-driven dynam-  
 442 ics at ganymede’s upstream magnetosphere: 3-d global hall mhd and mhd-  
 443 epic simulations. *Journal of Geophysical Research: Space Physics*, 125(8),  
 444 e2020JA028162.

445  
446  
447

Zhou, H., Tóth, G., Jia, X., Chen, Y., & Markidis, S. (2019). Embedded kinetic simulation of ganymede's magnetosphere: Improvements and inferences. *Journal of Geophysical Research: Space Physics*, 124(7), 5441–5460.

Author Manuscript